

# Appendix for “High-Dimensional Sensitivity Analysis for Genomic Studies: An Adversarial Framework for Learning Worst-Case Latent Confounders”

## S1 Data Availability

The systemic lupus erythematosus data (Perez et al., 2022), which we analyze in Section S10, is publicly available and can be downloaded at <https://www.ncbi.nlm.nih.gov/geo/query/acc.cgi?acc=GSE174188>. The Alzheimer’s dataset (Gabbitto et al., 2024) is publicly available and can be downloaded from <https://registry.opendata.aws/allen-sea-ad-atlas/>, and we focus on analyzing the microglial data from the prefrontal cortex.

## S2 Motivation for Confounder Modeling

The challenge of latent confounding is particularly acute in Alzheimer’s Disease (AD) research, where donors frequently exhibit complex comorbidity patterns or co-pathologies. Current computational methods struggle to isolate “direct” disease signals from these co-occurring processes.

**Comparison with Omitted Variable Bias (OVB) Frameworks.** Methods such as sensmaker (Cinelli & Hazlett, 2020) utilize partial  $R^2$  to reparameterize bias in linear models. While foundational, these approaches are not easily generalized to the non-linear Negative Binomial (NB) distributions required for pseudobulked single-cell RNA-seq data. sensGAN addresses this gap by enabling a formal sensitivity analysis across thousands of concurrent outcomes (genes) within a deep-learning adversarial framework.

**Comparison with Surrogate Variable Analysis (SVA)** : Standard genomic adjustment tools, including RUVr (Risso et al., 2014), CATE (Wang et al., 2017), GCATE (Du et al., 2025b), and causarray (Du et al., 2025a), focus on capturing residual variation through low-dimensional surrogates. While these provide explicit latent representations, they typically treat confounding as a fixed correction rather than a spectrum. Because these estimates are often independent of the treatment variable, they may fail to reflect biologically relevant latent factors—such as vascular disease or Lewy body pathology—that are statistically associated with both the AD case-control status and the observed gene expression matrix.

## S3 Details on Deviance, DBPR, and normalized predictive gains

In Section S3.1, we describe the four different models used in the calculation of the DBPR. In Sections S3.2 and S3.3, we formally define deviance and DBPR. In Section S3.4, we formally define the “knobs”  $\kappa$  and  $\eta$  used in sensGAN to quantify the predictive gain of a latent confounder.

### S3.1 Model family and fitted quantities.

For donors  $i \in \{1, \dots, n\}$ , let  $D_i \in \{0, 1\}$  denote treatment (i.e., case-control status),  $X_i \in \mathbb{R}^d$  observed covariates, and  $Y_{ij}$  the (pseudobulk) count for gene  $j \in \{1, \dots, p\}$ . For any candidate latent confounder matrix  $Z \in \mathbb{R}^{n \times k}$ , our generative family induces (i) a Bernoulli model for  $D$  with fitted linear predictor

$\pi$  (notation as in the main text), and (ii) a negative-binomial (NB) model for  $Y$  with fitted mean  $\mu$  and gene-specific dispersion  $\alpha$ . We write the corresponding log-likelihoods as  $\ell_D(\pi)$  and  $\ell_Y(\mu, \alpha)$ .

We instantiate the models in four standard ways for each task:

1. **Saturated model (sat):** The saturated models are the *perfect-fit* references that achieve the maximum possible log-likelihood. Denote these maxima by  $\ell_{D,\text{sat}}$  and  $\ell_{Y,\text{sat}}$ .
2. **Unadjusted model (un):** Fit models *without*  $Z$  to obtain  $(\hat{\pi}_{\text{un}}, \hat{\mu}_{\text{un}}, \hat{\alpha}_{\text{un}})$  and log-likelihoods  $\ell_D(\hat{\pi}_{\text{un}})$ ,  $\ell_Y(\hat{\mu}_{\text{un}}, \hat{\alpha}_{\text{un}})$ . In the following models, overdispersion is fixed at  $\hat{\alpha}_{\text{un}}$ .
3. **Most predictive confounder (Denoted by  $\hat{\cdot}$ ):** Define  $\hat{Z}$  as a confounder of dimension- $k$  that yields the best achievable fit when included in the models with unadjusted overdispersion  $\alpha$ , i.e., it maximizes the likelihood (equivalently minimizes deviance). After fitting, this produces  $(\hat{\pi}, \hat{\mu})$  and the log-likelihoods  $\ell_D(\hat{\pi})$ ,  $\ell_Y(\hat{\mu}, \hat{\alpha}_{\text{un}})$ .
4. **Arbitrary confounder (Denoted by  $\tilde{\cdot}$ ):** For any specific confounder  $\tilde{Z}$  (e.g., produced by sensGAN under constraints), fit models with the unadjusted overdispersion  $\alpha$  including  $\tilde{Z}$  to obtain  $(\tilde{\pi}, \tilde{\mu})$  and the log-likelihoods  $\ell_D(\tilde{\pi})$ ,  $\ell_Y(\tilde{\mu}, \hat{\alpha}_{\text{un}})$ .

### S3.2 Deviance

For modeling  $D$ , the Bernoulli deviance based on logits  $\text{Dev}_D \in \mathbb{R}$  is defined:

$$\text{Dev}_{\hat{D}_{\text{un}}} = \sum_{i=1}^n 2(\ell_{D_i,\text{sat}} - \ell_{D_i}(\hat{\pi}_{\text{un}})), \quad \text{Dev}_{\hat{D}} = \sum_{i=1}^n 2(\ell_{D_i,\text{sat}} - \ell_{D_i}(\hat{\pi})), \quad \text{Dev}_{\tilde{D}} = \sum_{i=1}^n 2(\ell_{D_i,\text{sat}} - \ell_{D_i}(\tilde{\pi})).$$

For modeling  $Y$ , the NB deviance  $\text{Dev}_Y = \{\text{Dev}_{Y_1}, \text{Dev}_{Y_2}, \dots, \text{Dev}_{Y_n}\} \in \mathbb{R}^n$  is the sum across genes:

$$\begin{aligned} \text{Dev}_{\hat{Y}_{\text{un}},i} &= \sum_{j=1}^p 2(\ell_{Y_{ij},\text{sat}} - \ell_{Y_{ij}}(\hat{\mu}_{ij,\text{un}}, \hat{\alpha}_{j,\text{un}})), \\ \text{Dev}_{\hat{Y}_i} &= \sum_{j=1}^p 2(\ell_{Y_{ij},\text{sat}} - \ell_{Y_{ij}}(\hat{\mu}_{ij}, \hat{\alpha}_{j,\text{un}})), \\ \text{Dev}_{\tilde{Y}_i} &= \sum_{j=1}^p 2(\ell_{Y_{ij},\text{sat}} - \ell_{Y_{ij}}(\tilde{\mu}_{ij}, \hat{\alpha}_{j,\text{un}})). \end{aligned}$$

Thus, deviance behaves like a likelihood-based error metric: lower deviance indicates a better fit.

### S3.3 DBPR: deviance-based partial $R^2$

We quantify the *incremental predictive gain* ( $R_D^2 \in \mathbb{R}$ ,  $R_Y^2 = \{R_{Y_1}^2, R_{Y_2}^2, \dots, R_{Y_n}^2\} \in \mathbb{R}^n$ ) of adding a confounder  $Z$  by the fraction of unadjusted deviance it removes.

Using the fitted models above, this yields the quantities shown in the main text:

$$\hat{R}_D^2 = \frac{\text{Dev}_{\hat{D}_{\text{un}}} - \text{Dev}_{\hat{D}}}{\text{Dev}_{\hat{D}_{\text{un}}}}, \quad \hat{R}_{Y_i}^2 = \frac{\text{Dev}_{\hat{Y}_{\text{un}},i} - \text{Dev}_{\hat{Y}_i}}{\text{Dev}_{\hat{Y}_{\text{un}},i}}, \quad \tilde{R}_D^2 = \frac{\text{Dev}_{\hat{D}_{\text{un}}} - \text{Dev}_{\tilde{D}}}{\text{Dev}_{\hat{D}_{\text{un}}}}, \quad \tilde{R}_{Y_i}^2 = \frac{\text{Dev}_{\hat{Y}_{\text{un}},i} - \text{Dev}_{\tilde{Y}_i}}{\text{Dev}_{\hat{Y}_{\text{un}},i}}.$$

### S3.4 Normalized DBPR (predictive-gain knobs)

Because  $\hat{Z}$  is defined to be the *most predictive* confounder in our model class,  $\hat{R}_D^2$  and  $\hat{R}_Y^2$  represent maximal attainable deviance reduction for predicting  $D$  and  $Y$ , respectively. We therefore define normalized predictive gains for any  $\tilde{Z}$  by

$$\kappa = \frac{\tilde{R}_D^2}{\hat{R}_D^2}, \quad \eta = \frac{\frac{1}{n} \sum_{i=1}^n \tilde{R}_{Y_i}^2}{\frac{1}{n} \sum_{i=1}^n \hat{R}_{Y_i}^2},$$

so that  $\kappa, \eta \in [0, 1]$  quantify the *fraction of maximal predictive gain* achieved by  $\tilde{Z}$  for  $D$  and  $Y$ .

## S4 SenGANS architectures

In Section S4.1, we discuss why we found it better to model latent confounders at the donor level (via pseudobulking the gene expression vectors) rather than at the cell level. In Section S4.2, we define the generator architecture used in sensGAN to compute the latent confounder for each donor.

### S4.1 Rationale for modeling scRNA-seq data on a donor level

We explain why we model sensGAN at the “donor level” (pseudobulking all cells from each of the  $n$  donors, despite having scRNA-seq data) rather than at the “cell level.” Specifically, this means we sum all the gene expression vectors of each cell to represent the gene expression vector for donor  $i$ , for  $i \in \{1, \dots, n\}$ . Our choice to pseudobulk the data might seem counterintuitive, since there are existing methods such as causarray (Du et al., 2025a) and CoCoA-diff (Park & Kellis, 2021) that model latent confounders at the cell level. However, we note some important distinctions that motivate our choice of pseudobulking the data, despite having scRNA-seq data:

- **Intended goal of adjusting for latent confounders that represent future neuropathologies:** As we mentioned in Section 1.1 in the main text, one of the primary motivations of sensGAN is to have the estimated latent confounders represent potential co-occurring neurodegenerative diseases. This is fundamentally a donor-level quantity. In contrast, methods such as causarray (Du et al., 2025a) and CoCoA-diff (Park & Kellis, 2021) learn cell-level confounders, which do not scientifically represent the same goal as our intended goal.
- **Considerations for the complexity of sensGAN architecture and computational efficiency:** Consider the architecture of the generator, which we describe in Section S4.2. If we model the data at the cell level, we would need to adjust the architecture so that the donor-level confounder can be “broadcasted” to all cells from that donor. While this is feasible, it would dramatically increase the computational burden of fitting sensGAN and, hence, be detrimental to the goal of learning latent confounders.

### S4.2 Generator architecture

The sigmoid-head generator directly maps the input to a bounded confounder via a deterministic neural network:

$$\begin{aligned} h &= \phi(W_1[X, D, Y] + b_1), \\ \tilde{Z} &= \sigma(W_2h + b_2), \end{aligned}$$

where  $\phi(\cdot)$  denotes a ReLU activation and  $\sigma(\cdot)$  is the elementwise sigmoid function. This parameterization produces  $\tilde{Z}$  deterministically and is simple and stable to optimize. In practice, we initialize the final-layer weights ( $W_2, b_2$ ) by fitting a ridge regression in logit space, so that  $\sigma(W_2h + b_2) \approx Z^{(0)}$ , where  $Z^{(0)}$  is an initial confounder estimate.

## S5 Loss details

Here, we include more details about the explicit calculations of the loss terms for the different components of sensGAN. In Section S5.1, we define the likelihood loss used in the treatment predictor and the outcome predictor. In Section S5.2, we define all the terms of the regularization term  $\mathcal{L}_{\text{reg}}$  used when training in the generator in the adversarial training step of sensGAN.

### S5.1 Likelihood Loss

For the treatment predictor  $f_D(\cdot)$ , we use the binary cross-entropy loss with logits. Let  $\hat{s}_i \in \mathbb{R}$  denote the predicted logit for donor  $i$ , and let  $\hat{\pi}_i = \sigma(\hat{s}_i)$  be the corresponding predicted treatment probability, where

$\sigma(\cdot)$  denotes the logistic function. The per-donor loss is given by

$$\ell_i^{\text{BCE}} = \max(\hat{s}_i, 0) - \hat{s}_i D_i + \log\left(1 + e^{-|\hat{s}_i|}\right),$$

which is a numerically stable implementation of binary cross-entropy with logits loss.

For the outcome predictor  $f_Y(\cdot)$ , we model gene expression counts with a negative binomial distribution. Let  $Y_{ij}$  denote the count for donor  $i$  and gene  $j$ , with mean  $\mu_{ij} > 0$  and dispersion  $\alpha_g > 0$ . Define  $r_j = 1/\alpha_j$ . The per-entry negative log-likelihood is

$$\ell_{ij}^{\text{NB}} = - \left[ \log \Gamma(Y_{ij} + r_j) - \log \Gamma(r_j) - \log \Gamma(Y_{ij} + 1) + r_j \log\left(\frac{r_j}{r_j + \mu_{ij}}\right) + Y_{ij} \log\left(\frac{\mu_{ij}}{r_j + \mu_{ij}}\right) \right].$$

We aggregate across genes to obtain a per-donor loss,

$$\ell_i^{\text{NB}} = \sum_{j=1}^p \ell_{ij}^{\text{NB}},$$

When training the most powerful predictor, the loss function used to train both  $f_D(\cdot)$  and  $f_Y(\cdot)$  is,

$$\mathcal{L}_L = \lambda_{\text{BCE}} \cdot \mathcal{L}_{\text{BCE}} + \lambda_{\text{NB}} \cdot \mathcal{L}_{\text{NB}}, \quad \text{where} \quad \mathcal{L}_{\text{BCE}} = \frac{1}{n} \sum_{i=1}^n \ell_i^{\text{BCE}}, \quad \mathcal{L}_{\text{NB}} = \frac{1}{n} \sum_{i=1}^n \ell_i^{\text{NB}}.$$

## S5.2 Regularization term

When training sensGAN via alternating adversarial optimization, we include a regularization term  $\mathcal{L}_{\text{reg}}$  to stabilize generator updates and prevent degenerate confounder solutions. Let  $\tilde{Z} \in \mathbb{R}^{n \times k}$  denote the current generator output and  $\hat{Z} \in \mathbb{R}^{n \times k}$  the strongest confounder used as a reference. The regularization consists of the following components.

The correlation regularizer

$$\mathcal{L}_{\text{corr}}(\tilde{Z}, \hat{Z}) = \frac{1}{k} \sum_{a=1}^k (1 - \text{Corr}(\tilde{Z}_{\cdot a}, \hat{Z}_{\cdot a}))^2 + \frac{1}{k(k-1)} \sum_{a \neq b} \text{Corr}(\tilde{Z}_{\cdot a}, \hat{Z}_{\cdot b})^2,$$

encourages each generated confounder dimension to align with its corresponding reference dimension while discouraging cross-dimensional mixing.

The cosine similarity regularizer

$$\mathcal{L}_{\text{cos}}(\tilde{Z}, \hat{Z}) = 1 - \frac{\langle \text{vec}(\tilde{Z}), \text{vec}(\hat{Z}) \rangle}{\|\text{vec}(\tilde{Z})\|_2 \|\text{vec}(\hat{Z})\|_2},$$

promotes global alignment between the generated and reference confounders up to scale.

Finally, the variance-matching regularizer

$$\mathcal{L}_{\text{var}}(\tilde{Z}, \hat{Z}) = \frac{1}{k} \sum_{a=1}^k \left( \text{Var}_n(\tilde{Z}_{\cdot a}) - \text{Var}_n(\hat{Z}_{\cdot a}) \right)^2$$

encourages the generated confounders to match the marginal scale of the reference confounder while preventing  $\tilde{Z}$  from collapsing to trivial or near-constant values.

We combine the regularizers into a single term,

$$\mathcal{L}_{\text{reg}} = \lambda_{\text{corr}} \cdot \mathcal{L}_{\text{corr}} + \lambda_{\text{cos}} \cdot \mathcal{L}_{\text{cos}} + \lambda_{\text{var}} \cdot \mathcal{L}_{\text{var}},$$

where  $\lambda_{\text{corr}}, \lambda_{\text{cos}}, \lambda_{\text{var}} \geq 0$  are tuning parameters.

## S6 Hyperparameters and training details

In Section S6.1, we document all the hyperparameters used in sensGAN. In Section S6.2, we describe in detail any additional training details of sensGAN not mentioned in the main text. In Section S6.3, we document the various ways we found empirically beneficial when post-processing the results after Step 2 of sensGAN (i.e., adversarially training the predictors and generator).

### S6.1 Hyperparameters for loss functions

**Optimization and training schedule.** sensGAN alternates between refitting two predictive models and updating a generator. All components are optimized using the Adam optimizer as implemented in PyTorch, using learning rates specified below; we use `zero_grad()` only to clear accumulated gradients between backpropagation steps.

**Predictor refitting.** At each outer iteration, we refit the treatment predictor  $f_D(\cdot)$  and the outcome predictor  $f_Y(\cdot)$  on the current generated confounder  $\tilde{Z}$ . For both predictors, `lr` denotes the optimizer learning rate, `epochs` the maximum number of training epochs, and `tol` a convergence tolerance used to stop training early when improvements fall below a threshold.

- **Treatment predictor  $f_D(\cdot)$ .** We train  $f_D$  with the binary cross-entropy loss with logits using a learning rate `lr_cls` =  $2 \times 10^{-1}$  and at most `epochs_cls` =  $10^4$  epochs. We use a validation split `split_cls` = 0.7 and early stopping with patience `patience_cls` = 200 and tolerance `tol_cls` =  $10^{-3}$ .
- **Outcome predictor  $f_Y(\cdot)$ .** We train  $f_Y$  by maximizing the negative binomial likelihood with a learning rate `lr_nb` =  $2 \times 10^{-1}$  and `epochs_nb` =  $10^3$  epochs.

**Generator updates.** The generator  $g(\cdot)$  is trained in an alternating fashion with the predictors. Training proceeds over `gen_steps` = 10 outer epochs. Within each outer epoch, the predictors are first refit on the current  $\tilde{Z}$ , after which the generator is updated for up to `epochs` = 100 gradient steps using Adam with learning rate `lr_gen` =  $10^{-3}$ .

**Generator loss weights.** We distinguish hyperparameters used for *predictor fitting* (above) from those used for the *generator objective*. In adversarial training, we penalize deviations from target predictive gains for  $D$  and  $Y$  with weights  $\lambda_D = 1$  and  $\lambda_Y = 1$ , and apply scaling factors  $s_D = s_Y = 10$  to normalize the magnitude of predictive-gain residuals. We additionally regularize the generator output to encourage structural alignment with the reference confounder via  $\mathcal{L}_{\text{corr}}$ ,  $\mathcal{L}_{\text{cos}}$ ,  $\mathcal{L}_{\text{var}}$  with weights  $\lambda_{\text{corr}} = \lambda_{\text{cos}} = \lambda_{\text{var}} = 10^{-3}$ . Unless otherwise stated, these hyperparameters are fixed across experiments and chosen for optimization stability rather than performance tuning.

### S6.2 Additional training details

**Initialization and warm start.** We initialize the generator by fitting  $g(\cdot)$  to reproduce the most powerful confounder  $\hat{Z}$ . We then warm-start the treatment and outcome predictors once using  $\hat{Z}$  before entering the outer training loop. No separate warmup stage is used beyond this initialization.

**Best-snapshot selection.** In practice, the alternating optimization may fail to simultaneously achieve the target predictive gains for both  $D$  and  $Y$  within a finite number of outer epochs. To ensure a stable and informative output in such cases, we track the generator state that attains the lowest total generator loss throughout training. Specifically, at each generator update, we record the current  $\tilde{Z}$  and associated statistics whenever the total loss improves upon the previously observed minimum. If the final training epochs do not meet the prescribed DBPR targets, we return the best-performing snapshot rather than the last iterate. This strategy prevents unstable late-stage updates from degrading the inferred confounder and provides a conservative estimate of the strongest confounder identified during training.

### S6.3 Post-processing of sensGAN results

**Calibration via leave-one-out predictive gains.** measured covariate. For each covariate  $X_i$ , we fit a leave-one-out (LOO) unadjusted NB GLM that excludes  $X_i$ , i.e.  $(X_{-i}, D) \rightarrow Y$ , and compare it to the corresponding unadjusted model that includes all measured covariates. The normalized predictive gain for outcome  $Y$ , i.e.  $\eta_{\text{LOO}}$ , is calculated based on these models, which captures the marginal predictive gain attributable to  $X_i$ . Repeating this procedure for all measured covariates yields an empirical distribution of  $\eta$ . We use this distribution as a calibration reference. Under the assumption that no latent confounder is stronger than a given measured covariate, we set the confounding strength parameter  $\eta$  (i.e., the confounding-effect knob) to match or remain below  $\eta_{\text{LOO}}$ .

**Selection for contour visualization.** For each target pair  $(\eta, \kappa)$ , sensGAN returns a generated confounder  $\tilde{Z}$  and the corresponding achieved predictive gains  $(\eta', \kappa')$ . Because alternating optimization may not exactly hit the prescribed targets, we apply a feasibility filter before constructing contour plots: we retain a run only if both gains are within a fixed tolerance,

$$|\eta' - \eta| \leq \epsilon \quad \text{and} \quad |\kappa' - \kappa| \leq \epsilon, \quad \text{where } \epsilon = 0.1.$$

Only feasible runs are included when aggregating statistics (e.g., significance counts or p-value summaries) over the  $(\eta, \kappa)$  grid; targets that fail this criterion are treated as missing and are not plotted.

**Isotonic smoothing.** To summarize trends as a function of predictive gain, we additionally apply an isotonic regression transform to obtain a monotone estimate of the relationship between  $-\log_{10} p$  and the achieved treatment gain  $\kappa'$ . Concretely, we fit a non-increasing isotonic regression model with clipping for out-of-range inputs,

$$\hat{m}(\cdot) = \text{IsoReg}(\text{decreasing}, \text{out\_of\_bounds} = \text{clip}).$$

Then, we report  $\hat{m}(\kappa')$  as the calibrated curve. This monotone post-processing reduces local noise across grid evaluations while preserving the expected directional effect.

**Refitting p-values for real data analyses.** For real-data applications (SLE in Section S10 and AD in Appendix Section S11), we refit the outcome models (`R:glmGamPoi`) using the inferred confounder  $\tilde{Z}$  to obtain final statistical significance measures. The refitting step yields calibrated p-values that account for overdispersion and mean-variance relationships in count data while decoupling statistical inference from the neural network training procedure.

## S7 sensGAN pseudocode

We present the pseudocode for sensGAN in Algorithm 1 to provide a high-level overview of its steps.

## S8 Data simulation details

In Sections S8.1 and S8.2, we describe how we simulated a binary and continuous-valued latent confounder  $Z$ , respectively. In Section S8.3, we document our crawler, which is used to compute the reference sensitivity contours. In Section S8.4, we document the results of how our crawler performed in our simulation setting.

### S8.1 Binary $Z$ simulation

We first describe the simulation used to generate the results shown in Figures 3 and 3 and Table 1 in the main text, where we demonstrated that sensGAN is able to accurately estimate the latent confounders based on  $(\kappa^*, \eta^*)$  and that the genes were appropriately partitioned into different categories based on whether or not they were associated with the latent confounders. Here, we simulate the measured covariate matrix  $X \in \mathbb{R}^{n \times d}$  and the latent binary confounder  $Z \in \mathbb{R}^{n \times k}$  independently. Then, we simulate the treatment  $D \in \mathbb{R}^{n \times 1}$  from a Bernoulli distribution with a logit link, while controlling for the variance contributed by

---

**Algorithm 1** sensGAN: adversarial sensitivity analysis with predictive-gain constraints

---

**Input:** Disease status  $D \in \{0, 1\}^n$ , covariates  $X \in \mathbb{R}^{n \times d}$ , pseudobulk counts  $Y \in \mathbb{N}^{n \times p}$ , confounder dimension  $k$ , targets  $\eta^* \in [0, 1]$ , training hyperparameters, significance level  $\delta$ , training tolerance  $\epsilon_\kappa, \epsilon_\eta \in (0, 1)$ .

**Output:** Worst-case confounders  $\{\hat{Z}(\kappa, \eta)\}$ , worst-case p-values  $\{\tilde{P}(\kappa, \eta)\}$ , and sensitivity contours.

- 1: **Step 1A: GLM unadjusted model.**
  - 2: Fit unadjusted GLM, regressing  $D$  onto  $X$ , to obtain fitted unadjusted logistic function  $\hat{\pi}_{\text{un}}$ .
  - 3: Fit unadjusted GLM, regressing  $Y$  onto  $(X, D)$  to obtain: (1) fitted unadjusted mean function  $\hat{\mu}_{\text{un}}$ , (2) overdispersions  $\hat{\alpha}_{\text{un}}$ , and (3) unadjusted standard errors  $\text{SE}(\hat{T}_{Y, \text{un}})$ .
  - 4: **Step 1B: Learn the most powerful confounder  $\hat{Z}$  (most predictive gain).**
  - 5: Initialize the weights for the treatment predictor  $f_D(\cdot) : \{X, Z\} \mapsto D$ , outcome predictor  $f_D(\cdot) : \{X, D, Z\} \mapsto Y$ , and generator  $g(\cdot) : \{X, D, Y\} \mapsto \hat{Z} \in (0, 1)^{n \times k}$ .
  - 6: **while** Repeat until convergence **do**
  - 7:     (a) **Predictors step:**
  - 8:         Train  $f_D(\cdot)$  with the current  $\hat{Z}$  to minimize  $\mathcal{L}_{\text{BCE}}$ .
  - 9:         Train  $f_Y(\cdot)$  with the current  $\hat{Z}$  to minimize  $\mathcal{L}_{\text{NB}}$ , using with overdispersions  $\hat{\alpha}_{\text{un}}$ .
  - 10:    (b) **Generator step:**
  - 11:         Train  $g(\cdot)$  to minimize  $\mathcal{L}_L = \lambda_{\text{BCE}} \cdot \mathcal{L}_{\text{BCE}} + \lambda_{\text{NB}} \cdot \mathcal{L}_{\text{NB}}$ .
  - 12: **end while**
  - 13: Compute the maximal DBPRs  $(\hat{R}_D^2, \hat{R}_Y^2)$  based on the most powerful confounder  $\hat{Z}$ .
  - 14: **Step 2: Worst-case confounder GAN under predictive-gain constraints.**
  - 15: Choose a sequence of values  $\mathcal{K} \subset [0, 1]$ .
  - 16: **for** fixed  $\eta$  and each  $\kappa \in \mathcal{K}$  **do**
  - 17:     Compute normalized predictive gains  $\kappa' = \tilde{R}_D^2 / \hat{R}_D^2$  and  $\eta' = \tilde{R}_Y^2 / \hat{R}_Y^2$ .
  - 18:     **while**  $|\kappa' - \kappa| > \epsilon$  **or**  $|\eta' - \eta| > \epsilon$  **do**
  - 19:         (a) **Predictor step (maximize log-likelihood):**
  - 20:             Train  $f_D(\cdot)$  with the current  $\tilde{Z}$  to minimize  $\mathcal{L}_{\text{BCE}}$ .
  - 21:             Train  $f_Y(\cdot)$  with the current  $\tilde{Z}$  to minimize  $\mathcal{L}_{\text{NB}}$ , using with overdispersions  $\hat{\alpha}_{\text{un}}$ .
  - 22:         (b) **Generator step (worst-case under constraints):**
  - 23:             Train  $g(\cdot)$  to minimize  $\mathcal{L}_S + \mathcal{L}_P + \mathcal{L}_{\text{reg}}$ , using significance level  $\delta$ , the unadjusted standard errors  $\text{SE}(\hat{T}_{Y, \text{un}})$ , the maximal DBPRs  $(\hat{R}_D^2, \hat{R}_Y^2)$ , and targets  $(\kappa, \eta)$ .
  - 24:     **end while**
  - 25:     Save the confounder  $\tilde{Z}$ , corresponding worst-case and p-values for all  $p$  genes corresponding to  $\kappa^*$ .
  - 26: **end for**
- 

terms involving  $X$  and  $Z$ . With the Negative Binomial GLM link function, we simulated the mean count matrix of scRNA-seq pseudocounts  $Y \in \mathbb{R}^{n \times p}$ . Then, we simulated the overdispersion rate to be a normal distribution centered around a constant vector  $C \in \mathbb{R}^{p \times 1}$ . Our simulated data can be compactly denoted as,

$$D \sim \text{Bernoulli}(\sigma(XB_D + Z\Gamma_D))$$
$$Y \sim \text{NB}(\log(\mu), \alpha), \text{ where } \log(\mu) = DT_Y + XB_Y + Z\Gamma_Y,$$

where  $\sigma(\cdot)$  denotes the sigmoid function.

With different combinations of  $T_Y \in \mathbb{R}^{1 \times p}$  and  $\Gamma_Y \in \mathbb{R}^{k \times p}$ , we simulated 3 categories of genes with varied significance profiles:

- **Category i (“Significant”):** Genes significantly associated with  $D$  but not with  $Z$ . Their expression remains significantly associated with  $D$  both with and without adjusting for  $Z$ . They are later referred to as the (always) significant genes.
- **Category ii (“Nullified”):** Genes significantly associated with  $Z$  but not with  $D$ . These genes appear significant without adjusting for  $Z$  but become insignificant once  $Z$  is included in the model. They are later referred to as the nullified genes.

- **Category iii (“Insignificant”)**: Genes not significantly associated with either  $D$  or  $Z$ . They remain insignificant with and without adjustment for  $Z$ . They are later referred to as the (always) insignificant genes.

In this simulation, we set  $n = 100$ ,  $p = 100$ ,  $d = 4$ ,  $k = 1$ ,  $C = 0.5$ .

## S8.2 Continuous $Z$ simulation for contour validation

Next, we describe the simulation used to generate Figure 5, which validates the contours of each gene. This simulation experiment validates the contour curves generated by sensGAN. Most simulation settings are similar to the above. The one difference is that we now simulate the continuous latent confounder  $Z \in (0, 1)^{n \times k}$ , where each entry is drawn independently and identically distributed from a uniform distribution. As mentioned in the main text, we use a continuous  $Z$  in this simulation to have finer control over predictive gains. In this experiment, we only simulated genes in **Category ii**, set  $n = 100$ ,  $p = 10$ ,  $d = 4$ ,  $k = 1$ ,  $C = 0.5$ . We use  $p = 10$  so our contour validation works better empirically (see Appendix Section S8.3 for details of our crawler) and so we can restrict attention to genes that are associated with  $Z$  but not with  $D$ . Although Category ii genes are simulated to be nullified by adjustment for  $Z$ , in practice, not all such genes are empirically nullified, since the outcome predictive gain of  $Z$  is constrained by the target  $\eta$  and finite-sample randomness can obscure marginal significance changes.

## S8.3 Crawler-based confounder generation.

To validate the contour generated by sensGAN, we implement a crawler-style worst-case search that directly explores the space of continuous confounders  $Z \in [0, 1]^n$ . This procedure is used to generate the *reference contours* shown in Figure 5 of the main text.

The crawler iteratively proposes candidate confounders using a diverse set of heuristics designed to cover a broad range of plausible confounding structures:

- **Independent random draws**: Sampling  $Z$  i.i.d. from  $\text{Uniform}(0, 1)$ .
- **Perturbations of the true confounder**: Adding noise to the simulated ground-truth  $Z$  to explore nearby confounding directions.
- **Rank-based transformations of  $D$** : Constructing  $Z$  from the ranks of the treatment assignment, optionally with added noise.
- **Rank-based transformations of  $Y$** : Using high-variance genes in  $Y$  to induce confounders correlated with outcome structure.
- **Principal components of  $(Y, D)$** : Extracting leading principal components from the concatenated matrix of outcomes and treatment.
- **Jittered refinements of previous candidates**: Locally perturbing previously evaluated confounders to refine coverage of promising regions.

Each proposed confounder  $Z$  is evaluated by refitting adjusted models for  $D$  and  $Y$  and computing the corresponding deviance-based partial  $R^2$  values. These are normalized to obtain predictive-gain coordinates  $(\kappa, \eta)$ . Candidates are then archived on a predefined  $(\kappa, \eta)$  grid, and for each grid cell, the crawler retains the confounder that minimizes the number of significant genes, yielding an explicit approximation to the worst-case confounding scenario.

## S8.4 Contour construction with crawler-based confounder.

To construct the reference contours, we discretize both  $\kappa$  and  $\eta$  into 11 equally spaced bins over  $[0, 1]$ , resulting in an  $11 \times 11$  grid (Fig. S1). Only confounders whose achieved predictive gains fall within the corresponding bin are used to summarize that grid cell.

Table S1 reports the number of candidate confounders evaluated by the crawler that fall into each  $\kappa$  bin ( $\pm 0.05$ ), illustrating coverage of the predictive-gain space.

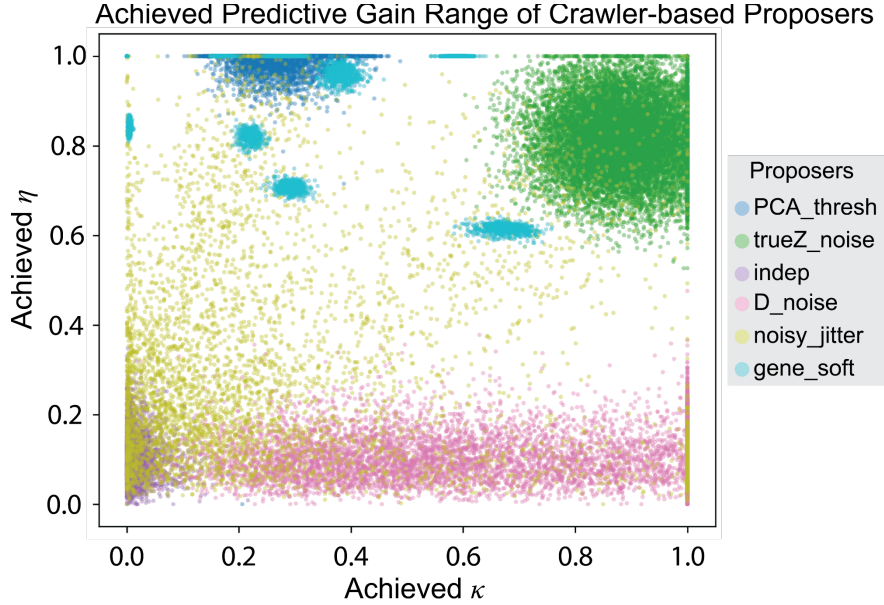


Figure S1: **Coverage of the  $(\kappa, \eta)$  predictive-gain space achieved by the crawler-based proposers.** Each point corresponds to a candidate confounder  $Z$  proposed by the crawler and evaluated by its normalized predictive gains for  $D$  ( $\kappa$ ) and  $Y$  ( $\eta$ ). Different proposal heuristics populate distinct regions of the grid, illustrating the heterogeneous and uneven coverage induced by direct search. This visualization motivates the need for sensGAN to more systematically and continuously explore the predictive-gain space.

Table S1: Number of crawler-generated confounders in each  $\kappa$  bin ( $\pm 0.05$ ).

$\kappa$ bin	0.0	0.1	0.2	0.3	0.4	0.5	0.6	0.7	0.8	0.9	1.0
Count	42	72	60	37	21	30	32	27	20	5	8

## S9 Additional Results: Simulation

To evaluate sensGAN at the gene level by comparing per-gene sensitivity contour curves, we further summarized gene-level behavior with a contingency table that classifies genes as always significant, nullified, or always insignificant (Table S2). The contingency analysis shows that sensGAN accurately recovers the nullification status for the majority of genes, with consistent agreement across all three categories.

Method	Category	Significant	Nullified	Insignificant
sensGAN	Significant	1	0	0
	Nullified	0	3	1
	Insignificant	0	0	5

Table S2: **Gene-level nullification agreement between the crawler reference and sensGAN.** The table reports the number of genes assigned to each significance category by sensGAN, stratified by the corresponding categories identified by the crawler-based reference. sensGAN correctly identifies 3 out of 4 genes that are nullified under worst-case confounding in the crawler analysis.

## S10 Additional Results: Systemic lupus erythematosus analysis

Systemic lupus erythematosus (SLE) is an autoimmune disease predominantly affecting women and individuals of Asian, African, and Hispanic descent (Perez et al., 2022). Multiplexed single-cell RNA sequencing was developed to capture the complexity of immune cell populations and systematically profile the composition and transcriptional states of immune cells in a large multiethnic cohort. Our goal for this analysis is to

demonstrate the rigor of sensGAN: withholding key donor covariates yields results similar to those from a differential expression analysis that uses them.

To remove genes with small variations, we preprocess the single-cell data by selecting the top 2,000 highly variable genes (HVGs) within each cell type, computing pseudobulk gene expression vector for each donor, and normalizing counts to the total library size per cell. With a focus on the T4 cell type, we aggregated single-cell expression profiles by summing counts across cells from the same subject, yielding a gene-level pseudobulk count matrix. Then, we removed genes with over 90% zero counts across subjects, retaining those expressed in at least 10% of donors for downstream analysis. To ensure method stability, we also removed genes whose counts didn't converge in the naive GLM Negative Binomial Model. In total, the dataset included  $n = 256$  subjects (158 cases and 98 controls). For each subject, the case-control variable represented systemic lupus erythematosus (SLE) status, and the final number of retained genes was  $p = 475$ .

In the proof-of-principle analysis, we only provide the method with sex ( $d = 1$ ) while holding out other measured covariates, including ethnicity and the sequencing batch information. To make sure the method captures biologically meaningful confounders, we decided to search for confounders ( $k = 3$ ) with a wider range of confounding effects by letting  $\kappa$  and  $\eta$  be equal to each other and vary together, i.e., letting  $Z$ 's predictive gains on  $Y$  be equal to  $Z$ 's predictive gains on  $X$ . With a series of  $(\kappa, \eta)$  values from 0.2 to 1, with a step size of 0.05, the method identified a series of confounders. We then performed adjusted differential expression analyses with confounders of varying strengths.

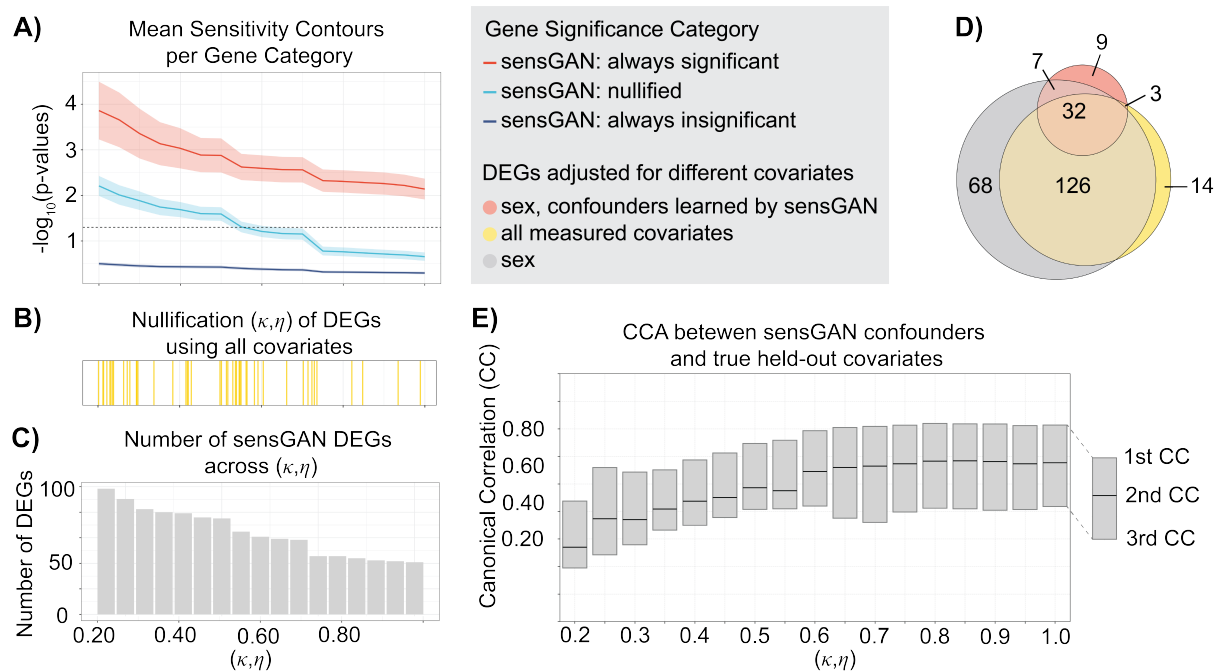


**Figure S2: sensGAN identifies robust SLE DEGs under increasing latent confounding and learns biologically meaningful confounders aligned with held-out covariates.** **A)** The sensitivity diagnostic contour plot with  $(\kappa, \eta)$ , where  $\kappa = \eta$ , varying from 0.2 to 1. **B)** The  $\kappa$  and  $\eta$  values where genes are nullified, extrapolated from the stepwise curve. **C)** The barplot of the number of DEGs at varying  $(\kappa, \eta)$  pairs. **D)** The Venn plot of significant DEGs calculated by the GLM Gamma-Poisson model adjusting for different covariates. **E)** The canonical correlations between the sensGAN confounders at varying levels of strength and the held-out covariates.

First, we analyzed the significance profiles of genes under varying levels of confounder strengths. In the sensitivity contour plot (Fig. S2A), mean contour curves and 95% confidence intervals were colored by genes that are always significant, nullified, and always insignificant. Then, we calculated the exact  $\kappa$  at which the gene became insignificant by extrapolating on the stepwise contour curve (Fig. S2B). Shown by the bar graph of the number of differentially expressed genes in the  $\kappa$ s, we also observed that larger  $\kappa$  generally corresponded to fewer differentially expressed genes (Fig. S2C). These results showed that the method can identify a series of confounders with varying strengths, and that more significant DEGs in the original model

became insignificant as  $\kappa$  increased.

Then, we analyzed the DEG sets across 3 methods to understand how sensGAN compares to existing methods while applying to real data. We use the Gamma-Poisson regression model to identify the DEGs associated with SLE, adjusting for different sets of covariates. First, for the sensGAN method, we adjusted for sex and the sensGAN-learned confounders. Second, for the all-covariate method, we adjusted for all measured covariates. Third, for the unadjusted method, we did not adjust for latent confounding but only adjusted for sex. We presented the results as a Venn diagram, in which circle areas correspond to the total number of DEGs identified while adjusting for different sets of covariates (Fig. S2D). The unadjusted DEG set was the largest, because it only adjusted for sex. The all-covariate DEG set was smaller than the unadjusted DEG set and larger than the sensGAN DEG set, due to its adjustment of other measured covariates. The sensGAN DEG set only includes the genes that are always significant with varying levels of confounding strengths; therefore, the smallest set, most of which were also identified by the other methods.

Lastly, we summarized the relationships between the confounders ( $k = 3$ ) learned by sensGAN and the held-out covariates ( $d' = 4$ ) using canonical correlation analyses (CCA) (Fig. S2E). Every bar corresponds to 3 canonical correlation (CC) values while comparing the held-out covariates and the learned confounders. We observed that all CCs increased as the confounding strengths increased from 0.2 to 1. Based on this observation, we believed that the method could learn a series of biologically meaningful confounders that became increasingly similar to the held-out covariates as we allowed stronger confounding effects.

## S11 Additional Results: Alzheimer’s disease (AD) analysis

In Section S11, we overview preliminary analyses that demonstrate how co-occurring neurodegenerative diseases has a clinical impact when studying Alzheimer’s disease. In Section S11.2, we provide additional results on our microglial analysis that supplement results in the main text.

### S11.1 Background on impact of co-occurring neurodegenerative disease on AD

One of the major computational obstacles to studying cellular changes in the brain during AD progression is that, when post-mortem brain tissue is sequenced, the donor often has co-occurring neurodegenerative diseases beyond AD (Nichols et al., 2023; McAleese et al., 2021). These co-occurring neurodegenerative diseases (i.e., “co-pathologies”) can confound existing single-cell analyses. For example, in late-onset AD, only 31% of cases are described with AD-specific signatures (Robinson et al., 2023). To illustrate, we perform a preliminary analysis of a cohort of 4,168 deceased donors from the National Alzheimer’s Coordinating Center (NACC), all of whom were staged for AD and 5 other co-pathologies (Fig. S1A). As the severity of AD increases, an increasing percentage of those donors have more co-pathologies. These co-pathologies have a potential clinical impact, shortening donors’ lifespans, even after adjusting for AD severity (Fig. S1B).

Although many of the cited studies, including our analysis shown in Fig. S1 on the NACC cohort, suggest that adjusting for co-occurring neurodegenerative disease is important to uncover the “pure” AD transcriptomic changes, the difficulty lies in the evolving definitions of these co-pathologies (Jack Jr et al., 2024). For instance, Figure S1C summarizes how, when some of the major currently used clinical co-pathology staging criteria were standardized for AD research (Mirra et al., 1991; Braak & Braak, 1991; Montine et al., 2012; Nelson et al., 2019). There are major updates in our clinical diagnosis of brain tissue roughly every 10 years as our scientific understanding of this disease evolves. Given this ever-changing landscape, how do we ensure that our single-cell findings today are robust to possible confounding co-occurring neurodegenerative disease that we might formalize in the future?

### S11.2 Results

We additionally investigate which microglial states harbor the DEGs (both nullified or always significant). While our sensGAN analysis was performed on the pseudobulk level, the localization to specific microglial states reveals the underlying biological mechanism (Prater et al., 2023). We first visualize the microglia in the SEA-AD cohort by the annotated microglial state (Fig. S4A). Then, we find that for both genes that were always significant regardless of  $\kappa$  (i.e., *LGALS3* and *ANXA2*) or nullified genes (i.e., *AQP9*, *AHNAK*), the elevated gene expression typically occurs in DAM and transitory microglia (Fig. S4B). This demonstrates

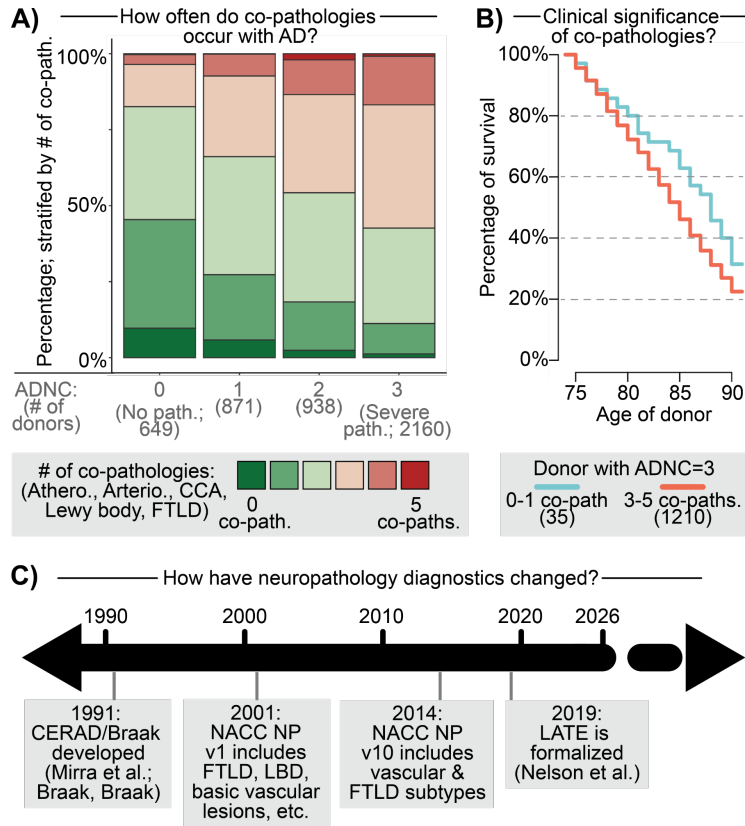


Figure S3: **Clinical impact of latent confounders in AD research and sensGAN overview to learn them.** **A)** Percentage of donors with number of co-occurring neurodegenerative disease, stratified by AD severity (ADNC score: 0 being no pathologies, 3 being severe). The number of donors in the NACC cohort in each stratum is marked. **B)** Survival curve among donors above the age of 75 with severe AD pathologies, stratified by whether they have 0/1 co-pathologies or 3+ co-pathologies. **C)** Timeline of when AD and related co-occurring neurodegenerative disease were standardized among clinical diagnostics of post-mortem brain tissue. **D)** Schematic sensGAN, showing that based on the donor covariates  $X$ , case-control  $D$  and pseudobulk RNA-seq profiles  $Y$ , sensGAN learns the worst-case confounders  $Z$  and confounder-adjusted p-values based two “knobs” which control the strength of latent confounders

the biological insight uniquely uncovered by sensGAN – although many of the originally implicated DEGs without any latent confounders are localized to DAM and transitory microglia, sensGAN enables us to further prioritize these DEGs based on how “pure” they are for microglia in AD.

## Appendix References

- Braak, H. and Braak, E. Neuropathological staging of Alzheimer-related changes. *Acta neuropathologica*, 82(4):239–259, 1991.
- Cinelli, C. and Hazlett, C. Making sense of sensitivity: Extending omitted variable bias. *Journal of the Royal Statistical Society Series B: Statistical Methodology*, 82(1):39–67, 2020.
- Du, J.-H., Shen, M., Mathys, H., and Roeder, K. Causal differential expression analysis under unmeasured confounders with causarray. *bioRxiv*, pp. 2025–01, 2025a.
- Du, J.-H., Wasserman, L., and Roeder, K. Simultaneous inference for generalized linear models with unmeasured confounders. *Journal of the American Statistical Association*, (just-accepted):1–24, 2025b.

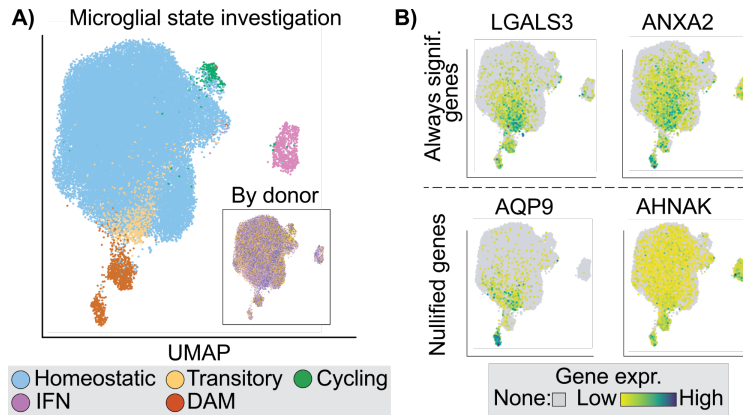


Figure S4: **sensGAN prioritizes DEGs specific to microglia in AD.** **A)** UMAP of single-nuclei microglia in SEA-AD, colored by microglial state and donor. **B)** Expression of certain genes across the microglia.

Gabitto, M. I., Travaglini, K. J., Rachleff, V. M., Kaplan, E. S., Long, B., Ariza, J., Ding, Y., Mahoney, J. T., Dee, N., Goldy, J., et al. Integrated multimodal cell atlas of Alzheimer's disease. *Nature Neuroscience*, 27(12):2366–2383, 2024.

Jack Jr, C. R., Andrews, J. S., Beach, T. G., Buracchio, T., Dunn, B., Graf, A., Hansson, O., Ho, C., Jagust, W., McDade, E., et al. Revised criteria for diagnosis and staging of Alzheimer's disease: Alzheimer's Association Workgroup. *Alzheimer's & Dementia*, 20(8):5143–5169, 2024.

McAleese, K. E., Colloby, S. J., Thomas, A. J., Al-Sarraj, S., Ansong, O., Neal, J., Roncaroli, F., Love, S., Francis, P. T., and Attems, J. Concomitant neurodegenerative pathologies contribute to the transition from mild cognitive impairment to dementia. *Alzheimer's & Dementia*, 17(7):1121–1133, 2021.

Mirra, S. S., Heyman, A., McKeel, D., Sumi, S., Crain, B. J., Brownlee, L., Vogel, F., Hughes, J., Belle, G. v., Berg, L., et al. The consortium to Establish a Registry for Alzheimer's Disease (cerad) Part ii. Standardization of the neuropathologic assessment of Alzheimer's disease. *Neurology*, 41(4):479–479, 1991.

Montine, T. J., Phelps, C. H., Beach, T. G., Bigio, E. H., Cairns, N. J., Dickson, D. W., Duyckaerts, C., Frosch, M. P., Masliah, E., Mirra, S. S., et al. National Institute on Aging–Alzheimer's Association guidelines for the neuropathologic assessment of Alzheimer's disease: A practical approach. *Acta Neuropathologica*, 123(1):1–11, 2012.

Nelson, P. T., Dickson, D. W., Trojanowski, J. Q., Jack, C. R., Boyle, P. A., Arfanakis, K., Rademakers, R., Alafuzoff, I., Attems, J., Brayne, C., et al. Limbic-predominant age-related TDP-43 encephalopathy (LATE): consensus working group report. *Brain*, 142(6):1503–1527, 2019.

Nichols, E., Merrick, R., Hay, S. I., Himali, D., Himali, J. J., Hunter, S., Keage, H. A. D., Latimer, C. S., Scott, M. R., Steinmetz, J. D., Walker, J. M., Wharton, S. B., Wiedner, C. D., Crane, P. K., Keene, C. D., Launer, L. J., Matthews, F. E., Schneider, J., Seshadri, S., White, L., Brayne, C., and Vos, T. The prevalence, correlation, and co-occurrence of neuropathology in old age: Harmonisation of 12 measures across six community-based autopsy studies of dementia. *The Lancet Healthy Longevity*, 4(3):e115–e125, 2023.

Park, Y. P. and Kellis, M. Cocoa-diff: Counterfactual inference for single-cell gene expression analysis. *Genome Biology*, 22(1):228, 2021.

Perez, R. K., Gordon, M. G., Subramaniam, M., Kim, M. C., Hartoularos, G. C., Targ, S., Sun, Y., Ogorodnikov, A., Bueno, R., Lu, A., et al. Single-cell RNA-seq reveals cell type-specific molecular and genetic associations to lupus. *Science*, 376(6589):eabf1970, 2022.

- Prater, K. E., Green, K. J., Mamde, S., Sun, W., Cochoit, A., Smith, C. L., Chiou, K. L., Heath, L., Rose, S. E., Wiley, J., et al. Human microglia show unique transcriptional changes in Alzheimer’s disease. *Nature Aging*, 3(7):894–907, 2023.
- Risso, D., Ngai, J., Speed, T. P., and Dudoit, S. Normalization of RNA-seq data using factor analysis of control genes or samples. *Nature Biotechnology*, 32(9):896–902, 2014.
- Robinson, J. L., Xie, S. X., Baer, D. R., Suh, E., Van Deerlin, V. M., Loh, N. J., Irwin, D. J., McMillan, C. T., Wolk, D. A., Chen-Plotkin, A., et al. Pathological combinations in neurodegenerative disease are heterogeneous and disease-associated. *Brain*, 146(6):2557–2569, 2023.
- Wang, J., Zhao, Q., Hastie, T., and Owen, A. B. Confounder adjustment in multiple hypothesis testing. *Annals of Statistics*, 45(5):1863, 2017.